Inorganic Chemistry

Article

pubs.acs.org/IC

Construction of Interpenetrated Ruthenium Metal–Organic Frameworks as Stable Photocatalysts for CO_2 Reduction

Shuquan Zhang, Lina Li, Sangen Zhao, Zhihua Sun, and Junhua Luo*

Key Laboratory of Optoelectronic Materials Chemistry and Physics, Fujian Institute of Research on the Structure of Matter, Chinese Academy of Sciences, Fuzhou, Fujian 350002, P. R. China

Supporting Information

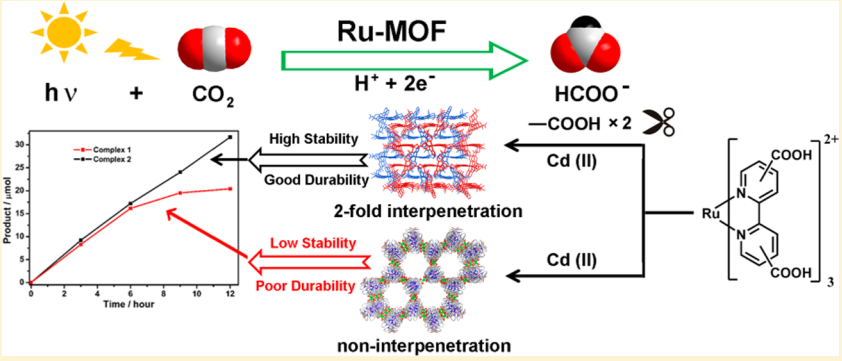

ABSTRACT: Poor stability has long been a major obstacle to the practical applications of metal–organic framework (MOF) photocatalysts. This problem can be overcome by the use of structural interpenetration. In this work, by modifying Ru metalloligands, we have rationally designed two Ru–polypyridine based MOFs (with non-interpenetrated and interpenetrated structures, respectively), both of which exhibit similar photocatalytic activities for CO_2 photoreduction. Remarkably, the interpenetrated Ru-MOF possesses good photocatalytic durability and recyclability, and shows much higher thermal and photic stability in comparison with its non-interpenetrated counterpart. To the best of our knowledge, this is the first time that the stability of MOF photocatalysts was improved by using structural interpenetration.

INTRODUCTION

Photocatalytic reduction of CO_2 to useful organic products is a highly appealing process owing to its significance for global energy and environmental issues.[1] Enormous efforts have been devoted to the development of effective photocatalytic materials, especially visible-light responsive photocatalysts, for CO_2 reduction.[2] In this respect, metal–organic frameworks (MOFs) are newly emerged but promising photocatalysts for CO_2 photoreduction,[3] mainly owing to their structural amenability to be designed with specific functionality. For example, modifying the amino groups on the organic linkers of some semiconductor-like MOFs, such as MIL-125(Ti) and Uio-66(Zr), can endow them with photocatalytic CO_2 reduction activities under visible-light irradiation.[3a,b] However, there still remains one major obstacle to the use of MOFs as photocatalyst, namely, their low stability; thus much more effort is still needed to push forward the development of stable MOF photocatalysts.

Until now, much attention has been paid to construction of stable MOFs, while very few examples have achieved the goal. Except for some extremely rigid MOFs based on high-oxidation-state metal species (such as Zr(IV) clusters)[4] or azole based ligands,[5] most MOFs are of high flexibility resulting in rather poor chemical and/or thermal stability, thereby limiting their photocatalytic applications. As we know, interpenetration, the entanglement of more than one isolated motifs, can effectively enhance the stability of the framework. For example, using interpenetration the groups of Zhou,[6a] Long,[6b] and Matsuda and Kitagawa[6c] constructed a series of robust MOFs with remarkable gas storage capacities. Recently, Zhang[7] et al. found that the interpenetration direction is more important than the interpenetration number for the porosity, stability, framework flexibility, and sorption behaviors of MOFs. Moreover, interpenetrated structures with good stability have also found wide use in many other important fields, such as molecular sensing and recognition[8] and selective catalytic reactions.[9] However, there is still a lack of studies on improving the stability of MOF photocatalysts through interpenetration.

Ru–polypyridine complexes are a class of highly photoactive materials with tremendously light-harvesting capacities and strong photoredox abilities. So they have long been applied as excellent photosensitizers and effective catalysts in homogeneous photocatalytic CO_2 reduction systems.[10] For example, Ishitani et al.[10a] recently reported a multinuclear Ru complex with the fastest reaction rate for visible light driven CO_2 photoreduction. Immobilization of such functional Ru com-

Received: May 10, 2015
Published: August 19, 2015

DOI: 10.1021/acs.inorgchem.5b01045
Inorg. Chem. 2015, 54, 8375–8379

plexes in the MOFs may render them effective heterogeneous photocatalysts for CO_2 photoreduction.

In this work, we rationally designed two Ru−polypyridine containing MOFs (with non-interpenetrated and interpenetrated structures, respectively), both of which can efficiently photochemically convert CO_2 to formate under visible-light irradiation. Remarkably, the interpenetrated Ru-MOF possesses good photocatalytic durability and recyclability, and shows much higher thermal and photic stability in comparison with its non-interpenetrated counterpart.

EXPERIMENTAL SECTION

Materials and Measurements. All reactants were reagent grade and used as purchased without further purification. Elemental analyses for C, H, N were carried out on a German Elementary Vario EL III instrument. The FT-IR spectra were performed on a Nicolet Magna 750 FT-IR spectrometer using KBr pellets in the range of 4000−400 cm^{-1}. The thermal decomposition behavior was analyzed by thermogravimetric analysis−mass spectrometry (TGA−MS) using a NETSCH STA-449C thermoanalyzer coupled with a NETSCH QMS403C mass spectrometer. The powder X-ray diffraction (PXRD) patterns were collected by a Rigaku DMAX2500 X-ray diffractometer using Cu Kα radiation (λ = 0.154 nm). Fluorescent analysis was performed on an Edinburgh Instruments FLS920 spectrofluorimeter equipped with both continuous (450 W) and pulsed xenon lamps. UV/visible absorbance was collected in an acetonitrile solution at room temperature on a PerkinElmer Lambda 650S UV/vis spectrometer equipped with Labsphere integrating over the spectral range 400−800 nm. The ^{13}C NMR spectra were measured using a Bruker AVANCE 400 spectrometer under the following conditions: acquisition time 2 s; 10500 times integration.

Synthesis of $\{Cd_3[Ru\text{-}L_1]_2\cdot 2(Me_2NH_2)\cdot solvent\}_n$, 1. The metalloligand $[Ru(5,5'\text{-dcbpy})_3]^{4-}$ ($[Ru\text{-}L_1]^{4-}$, 5,5′-dcbpy = 2,2′-bipyridine-5,5′-dicarboxylate) was synthesized by following the published procedure.[11] **1** was synthesized by a solvothermal method. A mixture of Ru complex (0.005 mmol, 5 mg) and $Cd(ClO_4)_2\cdot 6H_2O$ (0.02 mmol, 8 mg) was dissolved in 5 mL of DMF/H_2O solution in a 20 mL vial, and then was added 0.2 mL of perchloric acid (70% in water). The resulting solution was heated for 1.5 days at 100 °C. The product was obtained as needle shaped crystals (yield 82% based on Ru-H_6L). The phase purity of **1** was confirmed by comparing the powder X-ray diffraction (PXRD) patterns of the as-prepared sample and the simulated pattern from the crystal structure (Figure S1). Anal. Calcd for $C_{38}H_{26}O_{12}N_7RuCd_{1.5}$ (ignoring all of the solvent molecules): C 42.79, H 2.51, N 9.41%. Found (removing the solvent molecules in vacuum 80 °C, 18 h): C 42.57, H 2.61, N 9.28%. IR (cm^{-1}): 3425 (m, br), 3071 (w), 1617 (s), 1375 (s), 1121 (s), 1093 (m), 845 (w), 777 (m), 628 (m).

Synthesis of $\{Cd[Ru\text{-}L_2]\cdot 3(H_2O)\}_n$, 2. The precursor $Ru(4,4'\text{-}H_2dcbpy)_2Cl_2$ (4,4′-dcbpy = 2,2′-bipyridine-4,4′-dicarboxylate) was synthesized by following the published procedure.[12] Metalloligand $[Ru\text{-}L_2]^{2-}$ ($[Ru(4,4'\text{-dcbpy})_2(bpy)]^{2-}$, bpy = 2,2′-bipyridine) was in situ generated by $Ru(4,4'\text{-}H_2dcbpy)_2Cl_2$ and bpy ligand under hydrothermal reaction. **2** was synthesized by a hydrothermal reaction. A mixture of $Ru(H_2dcbpy)_2Cl_2$ (0.015 mmol, 10.5 mg), $Cd(ClO_4)_2\cdot 6H_2O$ (0.04 mmol, 16 mg), and bpy (0.06 mmol, 9.5 mg) was dissolved in 10 mL of deionized water solution in a 20 mL vial, and then the pH value was adjusted to ca. 10 by NaOH. The resulting solution was heated for 3 days at 180 °C. The product was obtained as block shaped crystals (yield 47% based on $Ru(H_2dcbpy)_2Cl_2$). The comparison of PXRD patterns of the as-prepared sample to the simulated pattern from the crystal structure suggested that the prepared crystals of **2** are of high purity (Figure S1). Anal. Calcd for $C_{34}N_6O_{11}H_{26}RuCd$: C, 44.97; H, 2.89; N, 9.25%. Found: C, 45.11; H, 2.74; N, 9.31%. Selected IR data (KBr pellet, cm^{-1}): 3421 (m, br), 3070 (w), 1629 (s), 1613 (s), 1541(s), 1469 (w), 1433 (m), 1404 (m), 1369 (s), 1026 (w), 863 (w), 781 (s), 711 (m), 663(w).

Photocatalytic Reaction. The visible light induced photocatalytic CO_2 reduction was performed in a 100 mL Schlenk tube with as-prepared samples. Photocatalyst (40 mg) enclosed in the tube was treated with vacuum and then purged with CO_2 several times. At the same time, a mixture of MeCN and triethanolamine (TEOA) (63 mL, 20/1 v/v) was degassed by CO_2 to remove dissolved O_2 and then injected into the reaction tube. The reaction was performed under the irradiation of a 500 W Xe lamp with a UV-cutoff filter to remove all wavelengths lower than 420 nm and an IR-cutoff filter to remove all wavelengths longer than 800 nm. The $HCOO^-$ formed was detected by ion chromatography (881 Compact IC pro, Metrosep) with Metrosep A supp 5 250/4.0 column. The column temperature was maintained at 303 K. The eluent is an aqueous solution of 3.2 mM Na_2CO_3 and 1.0 mM $NaHCO_3$.

RESULTS AND DISCUSSION

Single-crystal X-ray diffraction analysis revealed that Ru-MOF **1** crystallizes in the hexagonal space group *P6/mmm*, with 1/12 $[Ru\text{-}L_1]^{4-}$ metalloligand, 1/8 Cd(II) ion, and 1/12 dimethylamine cation in the asymmetric unit. The $Me_2NH_2^+$ counter-cations were generated from the decomposition of the DMF molecules. It is noticeable that the $[Ru\text{-}L_1]^{4-}$ metalloligand in the structure is disordered at two equivalent positions with the ratio of 1:1 (Figure S2). As shown in Figure 1a, each Cd(II) ion

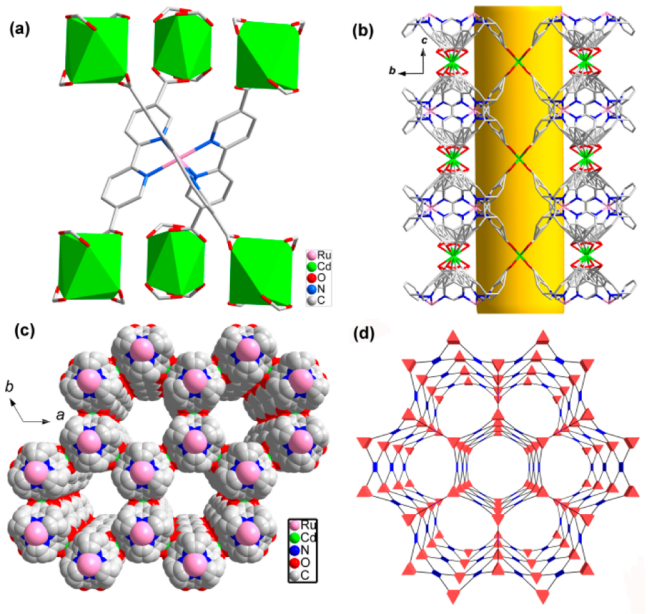

Figure 1. (a) Stick/polyhedra model showing the connectivity of metalloligand and Cd centers in **1**. (b) The 1D channel in **1** along the [001] direction. (c) Space-filling model of **1** viewed along the [001] direction. (d) Schematic showing **stp** topology of **1**. Hydrogen atoms are omitted for clarity.

adopts distorted bisdisphenoidal coordination geometry completed by four carboxylate groups from different metalloligands, serving as a square four-connected node. At the same time, the hexatopic $[Ru\text{-}L_1]^{4-}$ metalloligand was found to connect to six different Cd(II) centers, while acting as a six-connected node. As the result, the framework of **1** can be rationalized as a (4,6)-c **stp** network structure (Figure 1d). A view along the crystallographic *c* axis showed hexagonal one-dimensional channels with diameter 1.1 nm (Figure 1b,c). The solvent molecules within the channels were highly disordered. The potential solvent-accessible volume in compound **1** was estimated by PLATON[13] to be 58.0%.

DOI: 10.1021/acs.inorgchem.5b01045
Inorg. Chem. 2015, 54, 8375−8379

Although **1** possesses 1D channels with large void space, its channels are isolated by the enclosed channel walls, which obstruct the structural interpenetration. We hypothesized that decreasing the connectivity of $[Ru\text{-}L_1]^{4-}$ may open some windows on the channel walls and form 3D open channels, which may facilitate the framework interpenetration. To this end, we have designed a similar metalloligand, $[Ru\text{-}L_2]^{2-}$, with lower carboxylate density than $[Ru\text{-}L_1]^{4-}$ to build MOF with Cd(II) ions. Fortunately, we have successfully obtained an interpenetrated Ru-MOF **2**. **2** crystallizes in the monoclinic space group $P2_1/c$, as revealed by the single-crystal X-ray diffraction study. The asymmetric unit contains one $[Ru\text{-}L_2]^{2-}$ metalloligand, one Cd(II) ion, and three lattice water molecules. Each Cd(II) center coordinates to five oxygen atoms from four different $[Ru\text{-}L_2]^{2-}$ metalloligands (Figure 2a)

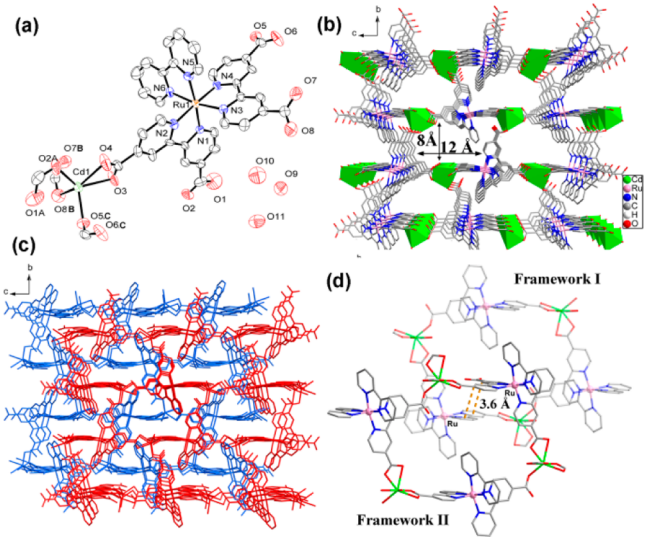

Figure 2. (a) The asymmetric unit of **2**. (b) View of a non-interpenetrated net in **2** along the [100] direction. (c) Stick model of the two interpenetrated nets in **2**. (d) The π-stacking interaction between neighboring nets in **2**. Hydrogen atoms are omitted for the clarity.

and thus acts as a four-connected node. Meanwhile, each $[Ru\text{-}L_2]^{2-}$ metalloligand links four separated cadmium(III) centers and can be considered as another four-connected node. Consequently, linking Cd(II) centers with $[Ru\text{-}L_2]^{2-}$ metalloligands result in a known but rare **lon** network structure (Figure S4). Generally speaking, the net topology plays a highly important role in structural interpenetration. To the best of our knowledge, diamond net is one of the most classic 4-c topologies, which involves various interpenetrated architectures.[14] As a diamond analogue net, **lon** net may also serve as a wonderful platform for structural interpenetration. As expected, the single **lon** type framework of **2** exhibits large 3D void space (Figure 2b, potential solvent-accessible volume is 61.3% for a single framework) which readily accommodates a second framework via interpenetration, leading to a 2-fold interpenetrating structure for **2** (Figure 2c). As depicted in Figure 2d, the two interpenetrated frameworks are stabilized by the strong π-stacking interactions between the $dcbpy^{2-}$ ligands of the neighboring nets.

The solid-state absorption spectra demonstrate that both **1** and **2** exhibit very broad absorption bands between 400 and 650 nm (Figure 3a). These absorption bands may be assigned

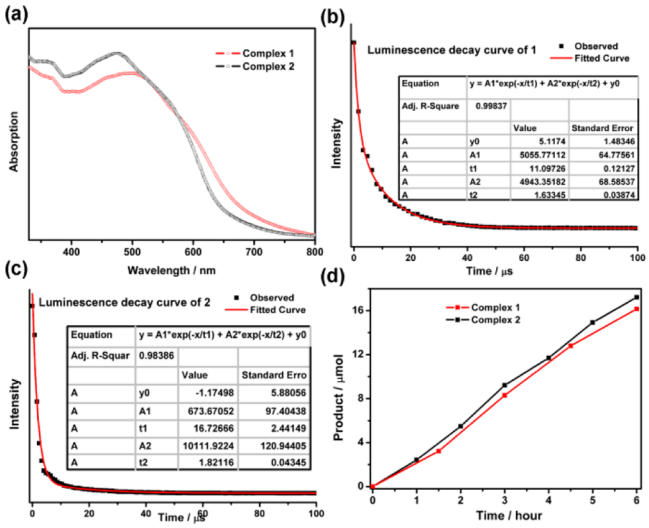

Figure 3. (a) The solid-state absorption spectra of **1** and **2**. (b, c) Luminescence decay curves of **1** and **2**, respectively. (d) Amounts of $HCOO^-$ generated from CO_2 as a function of irradiation time over photocatalysts. Solutions were under irradiation of Xe lamp with filters producing light in the range of 420−800 nm. Photocatalyst: 40 mg. MeCN/TEOA (vol:vol = 20/1). Solution volume: 60 mL.

to the singlet metal-to-ligand charge transfer (^{1}MLCT) of Ru metalloligands. These results are consistent with the previous reports by Lin, Kobayashi, and Kato et al.[15] In addition, **1** and **2** display long luminescence decay lifetime. As shown in Figure 3b,c, the luminescence decay of **1** and **2** is well fitted to the biexponential curve with the lifetime of 4.98 and 6.45 μs, respectively. Both the high light harvesting in visible-light region and long excited-state lifetimes of **1** and **2** are profitable for their applications in visible light induced photocatalysis.

To evaluate the potential of **1** and **2** in photocatalytic applications, we investigate their photochemical activities by the photocatalytic reduction of CO_2 under visible-light irradiation. The CO_2 photoreduction reactions were carried out using prepared samples of **1** and **2** as heterogeneous photocatalyst along with the sacrificial agent, triethanolamine (TEOA), under 420−800 nm light irradiation. The amounts of the photocatalytic product ($HCOO^-$) with increasing irradiation time are shown in Figure 3d. It became clear that complexes **1** and **2** exhibited similar photocatalytic activities for $HCOO^-$ generation, showing the $HCOO^-$ production of 16.1 and 17.2 μmol in 6 h, respectively. The quantum yield of $HCOO^-$ reached 0.51% and 0.54% for **1** and **2** with 475 nm light irradiation. The product formation rate $R_{product}$ was calculated as 67.5 and 71.7 μmol (g of catalyst)$^{-1}$ h^{-1} for **1** and **2**. These values are higher than those for previously reported photoactive MOFs, such as NH_2-MIL-125(Ti) and NH_2-Uio-66(Zr) (the R_{HCOO^-} of these photocatalysts are 16.3, and 26.4 μmol (g of catalyst)$^{-1}$ h^{-1}, respectively), and some visible-light responded semiconductors, such as iodide doped TiO_2 and nitrogen and nickel codoped TiO_2 ($R_{product}$ = 2.4 and 15.1 μmol (g of catalyst)$^{-1}$ h^{-1}, respectively).[3a,b,16] The similar but remarkable photocatalytic performance of **1** and **2** may be attributed to the immobilized highly light harvesting Ru units in the complexes which endow them with prominent photosensitive and catalytic abilities. But the photocatalytic activity of the nanoflowers is moderately lower than that of our recently reported Ir-CP[3c] with R_{HCOO^-} 118.8 μmol (g of catalyst)$^{-1}$ h^{-1}, which may be attributed to the more reductive unit $[Ir(ppy)_2(bpy)^+]$ units[17]

DOI: 10.1021/acs.inorgchem.5b01045
Inorg. Chem. 2015, 54, 8375−8379

(ppy = 2-phenylpyridine, bpy = 2,2′-bipyridine) immobilized in the Ir-CP. Furthermore, the supernatants were reused for the CO_2 reduction reaction under identical reaction conditions except without the photocatalysts. No additional $HCOO^-$ was detected, which approved the heterogeneous nature of the photocatalytic systems. Meanwhile, a series of controlled experiments of CO_2 photoreduction including in the dark, without Ru-MOFs, and without CO_2 were performed. No $HCOO^-$ was generated under all of these conditions. Controlled experiments using isotopic $^{13}CO_2$ were performed to verify the source of the produced $HCOO^-$. The $HCOO^-$ generated was analyzed by ^{13}C NMR spectroscopy. After 6 h reaction, the peaks at 164.82 ppm (for **1**) and 165.01 (for **2**) were assigned to $H^{13}COO^-$ (Figures S6 and S7). All these results confirmed that both **1** and **2** can indeed convert CO_2 to $HCOO^-$ via a visible light induced photocatalytic reaction.

Prolonged photocatalytic reactions had also been performed over a period of 12 h to investigate the photostability of **1** and **2**. As shown in Figure 4a, complex **2** maintained its photocatalytic activity in the second 6 h of reaction time; however, complex **1** gradually became inactive during the same period. To find out the reason for these distinct differences between the photocatalytic performances of **1** and **2**, we monitored their crystalline states and morphologies during the reaction by PXRD and SEM images. PXRD analysis indicated that complex **2** showed no structural change after 12 h of reaction time, but complex **1** lost its long-ranged ordered structure (Figure 4c,d). Meanwhile, the SEM images showed that the morphologies of **1** gradually changed from regular sheets to amorphous particles which are consistent with the mudlike feature of the **1** after the reaction. On the contrary, complex **2** maintained its lamellar morphology during the photocatalytic reaction. These results suggested that the structure of **2** is stable to the photocatalytic reaction, whereas the framework of **1** was collapsed. The Ru leakages from the photocatalysts were also consistent with the above-mentioned results. During the reactions, the clear supernatant solutions were monitored by ICP-OES analysis at different periods of time (Figure 4b). The Ru concentration in the system catalyzed by **1** increased much faster than that in the system catalyzed by **2**, indicating more Ru ions or units leaked from **1** than **2**. These experiments indicated that complex **2** has a better photostability than **1**.

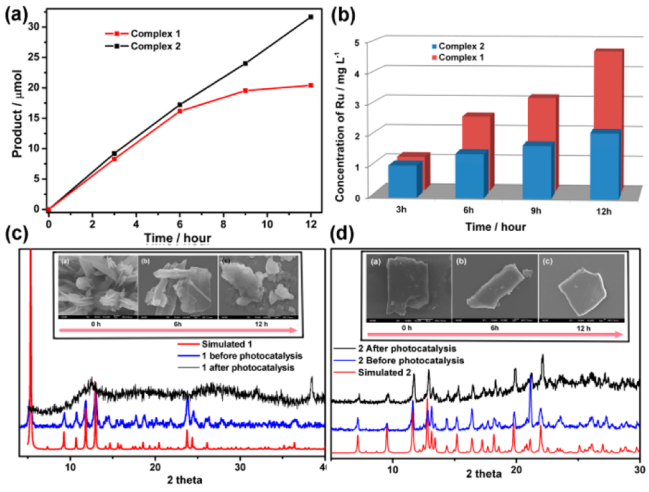

Figure 4. (a) Amounts of $HCOO^-$ generated from CO_2 as a function of irradiation time over photocatalysts. The reaction conditions were identical with the previous illustration, except that the reaction solution was bubbled with CO_2 after 6 h of reaction. (b) The Ru concentration in the reaction solution monitored at different reaction times. The PXRD patterns of **1** (c) and **2** (d) after photocatalysis (black), fresh samples (blue), and simulated (red).

The remarkable decrease in the photocatalytic activity of **1** may be attributed to its structural photodecomposition, which resulted in the morphological and chemical changes in the photocatalysts and finally decreased the catalytic and photosensitive abilities. The poor photostability of **1** may be closely associated with their structural stabilities. As mentioned above, complex **1** features a porous framework with large void space. Except for the coordination between metal ions and ligands, the framework of **1** is supported by the supramolecular interactions between the framework and the guest molecules filled in the channels. Under the photocatalytic condition, the guest molecules will exchange with the solvent molecules, which may weaken the supramolecular interactions and lead to the structural collapse. On the contrary, besides the coordination interaction, the interpenetrated frameworks also effectively stabilize the structure of **2** by strong π-stacking interactions between the adjacent nets. Hence **2** possesses superior structural stability which endows it with commendable photostability to the photoredox chemistry system.

The outstanding structural stability of **2** was also confirmed by the thermogravimetric analysis (TGA) studies on complexes **1** and **2**. As shown in Figure 5, the framework of **1** begins to decompose at about 170 °C. On the contrary, complex **2** is much more stable and maintains its structural stability up to about 280 °C, which can be confirmed by the PXRD analysis of heat-treated samples (Figure S10). Compound **2** maintained its crystalline phase even treated at 280 °C, however, crystals of **1** transformed to an amorphous phase only treated at 60 °C. This phenomenon may be attributed to the enhanced rigidity of the structure by the means of interpenetration, which is also observed in many interpenetrated MOFs.[6c,18]

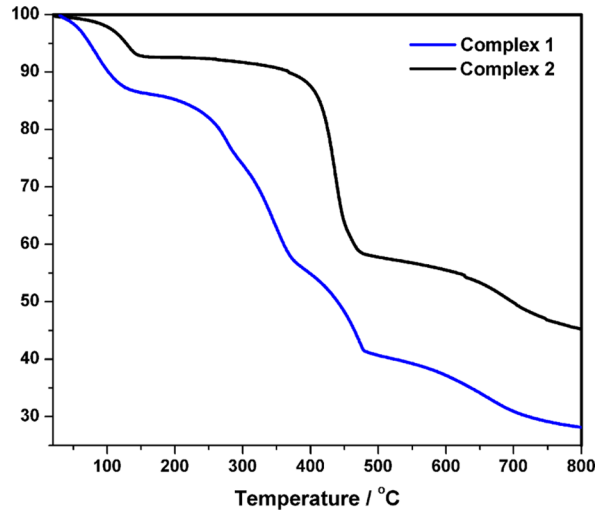

Figure 5. TGA curves of complexes **1** and **2**.

In view of the prominent stability of **2**, we tested the recyclability of this photocatalyst in photocatalytic CO_2 reduction. The photocatalyst in the reaction mixture was recovered and reused in the next repetitive photocatalytic reaction. The photocatalyst kept its intrinsic catalytic activity

DOI: 10.1021/acs.inorgchem.5b01045
Inorg. Chem. 2015, 54, 8375−8379

for four repetitions of 6 h reaction (Figure 6), indicating that **2** can be an effective heterogeneous photocatalyst with

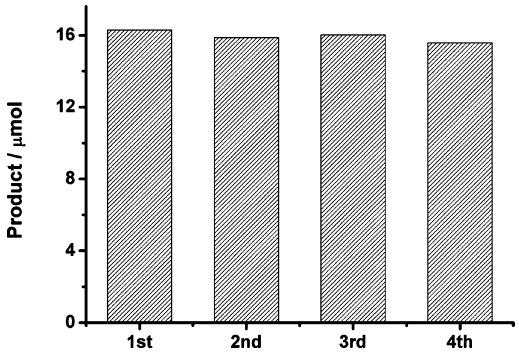

Figure 6. Recyclability of **2**. The amount of $HCOO^-$ generated in four repeats of photocatalytic operations.

remarkable photostability for CO_2 photoreduction. Consequently, an interpenetrated structure may be of great benefit to a heterogeneous photocatalyst with extraordinary photostability.

CONCLUSION

In summary, by rationally designing the Ru metalloligands, we have successfully synthesized two Ru−polypyridine based MOFs with non-interpenetrated and 2-fold interpenetrated structures, respectively. The interpenetrated Ru-MOF exhibits not only remarkable thermal stability but also superior photostability for photocatalytic CO_2 reduction as compared to its non-interpenetrated counterpart. The improved stability of the interwoven frameworks originates from the numerous interframework supramolecular interactions that prevent single net from collapsing in. These findings indicate that making interpenetration could be an effectively strategy to fabricate highly stable MOF photocatalysts.

ASSOCIATED CONTENT

Supporting Information

The Supporting Information is available free of charge on the ACS Publications website at DOI: 10.1021/acs.inorgchem.5b01045.

Detailed thermogravimetric analysis, ^{13}C NMR spectra, and figures (PDF)
Crystal data for **1** (CIF)
Crystal data for **2** (CIF)

AUTHOR INFORMATION

Corresponding Author

*E-mail: jhluo@fjirsm.ac.cn. Fax: (+86) 591-63173127. Tel: (+86) 591-63173126.

Notes

The authors declare no competing financial interest.

ACKNOWLEDGMENTS

This work was financially supported by NSFC (21222102, 21373220, 51402296, 21171166, and 21301172), the 973 Key Program of MOST (2011CB935904), and the NSF for Distinguished Young Scholars of Fujian Province (2014J06015). Z.S. and S.Z. are thankful for the support from "Chunmiao Projects" of Haixi Institute of Chinese Academy of Sciences (CMZX-2013-002 and CMZX-2015-003). L.L. is thankful for the support from "Youth Innovation Promotion Association CAS". Prof. Z. Li and Dr. D. Sun at Fuzhou University and Mr. Lin at Minjiang University are thanked for their help with the detection of $HCOO^-$ produced.

REFERENCES

(1) (a) He, M.; Sun, Y.; Han, B. *Angew. Chem., Int. Ed.* **2013**, *52*, 9620−9633. (b) Lanzafame, P.; Centi, G.; Perathoner, S. *Chem. Soc. Rev.* **2014**, *43*, 7562−7580.
(2) (a) Sato, S.; Morikawa, T.; Saeki, S.; Kajino, T.; Motohiro, T. *Angew. Chem., Int. Ed.* **2010**, *49*, 5101−5105. (b) Kondratenko, E. V.; Mul, G.; Baltrusaitis, J.; Larrazábal, G. O.; Pérez-Ramírez, J. *Energy Environ. Sci.* **2013**, *6*, 3112−3135.
(3) (a) Fu, Y.; Sun, D.; Chen, Y.; Huang, R.; Ding, Z.; Fu, X.; Li, Z. *Angew. Chem., Int. Ed.* **2012**, *51*, 3364−3367. (b) Sun, D.; Fu, Y.; Liu, W.; Ye, L.; Wang, D.; Yang, L.; Fu, X.; Li, Z. *Chem. - Eur. J.* **2013**, *19*, 14279−14285. (c) Li, L.; Zhang, S.; Xu, L.; Wang, J.; Shi, L.; Chen, Z.; Hong, M.; Luo, J. *Chem. Sci.* **2014**, *5*, 3808−3813. (d) Wang, C.; Zhang, Y.; Li, J.; Wang, P. *J. Mol. Struct.* **2015**, *1083*, 127−136. (e) Zhang, S.; Li, L.; Zhao, S.; Sun, Z.; Hong, M.; Luo, J. *J. Mater. Chem. A* **2015**, *3*, 15764−15768.
(4) (a) Feng, D.; Wang, K.; Su, J.; Liu, T.; Park, J.; Wei, Z.; Bosch, M.; Yakovenko, A.; Zou, X.; Zhou, H. *Angew. Chem., Int. Ed.* **2015**, *54*, 149−154. (b) Feng, D.; Chung, W.; Wei, Z.; Gu, Z.; Jiang, H.; Chen, Y.; Darensbourg, D. J.; Zhou, H. *J. Am. Chem. Soc.* **2013**, *135*, 17105−17110.
(5) Banerjee, R.; Phan, A.; Wang, B.; Knobler, C.; Furukawa, H.; O'Keeffe, M.; Yaghi, O. M. *Science* **2008**, *319*, 939−943.
(6) (a) Ma, S.; Sun, D.; Ambrogio, M.; Fillinger, J. A.; Parkin, S.; Zhou, H. *J. Am. Chem. Soc.* **2007**, *129*, 1858−1859. (b) Dincă, M.; Dailly, A.; Tsay, C.; Long, J. R. *Inorg. Chem.* **2008**, *47*, 11−13. (c) Bureekaew, S.; Sato, H.; Matsuda, R.; Kubota, Y.; Hirose, R.; Kim, J.; Kato, K.; Takata, M.; Kitagawa, S. *Angew. Chem., Int. Ed.* **2010**, *49*, 7660−7664.
(7) He, C.; Liao, P.; Zhou, D.; Wang, B.; Zhang, W.; Zhang, J.; Chen, X. *Chem. Sci.* **2014**, *5*, 4755−4762.
(8) Takashima, Y.; Martínez, V. M.; Furukawa, S.; Kondo, M.; Shimomura, S.; Uehara, H.; Nakahama, M.; Sugimoto, K.; Kitagawa, S. *Nat. Commun.* **2011**, *2*, 168.
(9) Song, F.; Wang, C.; Falkowski, J. M.; Ma, L.; Lin, W. *J. Am. Chem. Soc.* **2010**, *132*, 15390−15398.
(10) (a) Tamaki, Y.; Morimoto, T.; Koike, K.; Ishitani, O. *Proc. Natl. Acad. Sci. U. S. A.* **2012**, *109*, 15673−15678. (b) Kuramochi, Y.; Kamiya, M.; Ishida, H. *Inorg. Chem.* **2014**, *53*, 3326.
(11) Matthews, C. J.; Elsegood, M. R. J.; Bernardinelli, G.; Clegg, W.; Williams, A. F. *J. Chem. Soc., Dalton Trans.* **2004**, 492−497.
(12) Eskelinen, E.; Luukkanen, S.; Haukka, M.; Ahlgrén, M.; Pakkanen, T. A. *J. Chem. Soc., Dalton Trans.* **2000**, 2745−2752.
(13) Spek, A. L. *PLATON, A Multipurpose Crystallographic Tool*; Utrecht University: Utrecht, The Netherlands, 2008.
(14) Li, D. S.; Wu, Y. P.; Zhao, J.; Zhang, J.; Lu, J. Y. *Coord. Chem. Rev.* **2014**, *261*, 1−27.
(15) (a) Kent, C. A.; Mehl, B. P.; Ma, L. Q.; Papanikolas, J. M.; Meyer, T. J.; Lin, W. *J. Am. Chem. Soc.* **2010**, *132*, 12767−12769. (b) Kobayashi, A.; Ohba, T.; Saitoh, E.; Suzuki, Y.; Noro, S.; Chang, H.; Kato, M. *Inorg. Chem.* **2014**, *53*, 2910−2921.
(16) (a) Fan, J.; Liu, E.; Tian, L.; Hu, X.; He, Q.; Sun, T. *J. Environ. Eng.* **2011**, *137*, 171−176. (b) Zhang, Q.; Li, Y.; Ackerman, E. A.; Gajdardziska-Josifovska, M.; Li, H. *Appl. Catal., A* **2011**, *400*, 195−202.
(17) (a) Campagna, S.; Puntoriero, F.; Nastasi, F.; Bergamini, G.; Balzani, V. *Top. Curr. Chem.* **2011**, *303*, 151−184. (b) Dixon, I. M.; Collin, J. P.; Sauvage, J. P.; Flamigni, L.; Susana, E.; Barigelletti, F. *Chem. Soc. Rev.* **2000**, *29*, 385−391.
(18) Jiang, H.; Tatsu, Y.; Lu, Z.; Xu, Q. *J. Am. Chem. Soc.* **2010**, *132*, 5586−5587.

DOI: 10.1021/acs.inorgchem.5b01045
Inorg. Chem. 2015, 54, 8375−8379